Regular Article

ANALYTICAL
AND BIOANALYTICAL
CHEMISTRY
RESEARCH

Published by the
Iranian Chemical Society

***Anal. Bioanal. Chem. Res.**, Vol. 11, No. 1, 31-39, January 2024.*

Hybrid Aptamer-Molecularly Imprinted Polymer: Synergistic Recognition and Ultrasensitive Detection of Helicobacter Pylori

Mahmoud Roushani*, Masoumeh Sarabaegi and Hadi Hosseini

Department of Chemistry, Ilam University, P. O. Box: 69315-516, Ilam, Iran

(Received 24 July 2023, Accepted 30 October 2023)

The combination of aptamer is performed with molecularly imprinted (MIP) using their unique features. In this sense, first, the screen-printed carbon electrode (SPCE) was modified with nano-size iridium copper on nitrogen-doped carbon nanocapsoul (CN@IrCu), and, then, the Aptamer-MIP hybrid was used to detect *Helicobacter pylori*. This design leads to the use of dual properties of Aptamer and MIP. Moreover, CN@IrCu has been used as a substrate to increase aptamer loading and conductivity. The sensor shows a linear range from 10^2 CFU ml^{-1} to 10^7 CFU ml^{-1} with a detection limit of 33 CFU ml^{-1}. This Aptamer-MIP/CN@IrCu/SPCE was successfully evaluated in determining the concentration of *Helicobacter pylori* in blood serum samples with high reproducibility and selectivity.

Keywords: Molecularly imprinted polymers, Screen printed carbon electrode, Aptamer, *Helicobacter pylori*, Aptamer-MIP

INTRODUCTION

Electrochemical detection sensors, due to their simplicity, cheapness, rapid analysis capability, and short detection time, have received a lot of attention for the quantitative detection of different analytes [1]. One of the designs for the electrochemical sensor is the use of a screen-printed carbon electrode (SPCE) that has some specific advantages such as easy manufacturing method, portability, low cost, reliability in determining different materials, and flexibility in design. Moreover, the electrode surface can be easily modified with new materials to achieve a variety of improvements [2]. Therefore, due to the advantages and effective performance of SPCE, it has become very popular in the biomedical, environmental, and other major fields of analytical chemistry [3].

The MIP has very good physical and chemical stability with various analytes [4-7]. The MIP has several advantages as compared to aptamers, such as high physical/chemical stability, resistance, low cost of preparation, and high selectivity [8-14]. The MIP was used in solid phase extraction [15] and catalysis [16], sensing [17], separations [18] and drug delivery [19]. However, there are some disadvantages, such as poor bonding, slow mass transfer process, incomplete mold removal, and limited use in electrochemical sensors [20-22].

Aptamers have several advantages, including excellent interaction with nanomaterials, high selectivity, specific to bacteria and viruses, excellent stability, *etc*. [23]. The design of aptasensors has been considered in food science, medicine, etc., but aptamers are degraded under special conditions such as strong acids, and very high temperatures, so their use is limited [24-25].

To overcome the disadvantages of aptamer and MIP, the hybrid of the two can be used together and their advantages are doubled [26]. This strategy promises to produce aptamer-MIP with superior connectivity features [27]. Aptamer has been used as a bioreceptor in this approach [28]. Therefore, the combination of aptamer and MIP creates a connection with high selectivity.

The design and synthesis of metal nanosheets on carbon nanostructures have attracted much attention due to their

*Corresponding author. E-mail: m.roushani@ilam.ac.ir

unique physicochemical properties and inherent holes for aptamer loading in the Aptamer-MIP. In this research, we made a new composite of nano IrCu on nitrogen-doped carbon nanocapsules (CN@IrCu). The structure of hollow nanomaterials was completely characterized by various techniques of physical and chemical properties. This shell array with nano IrCu structures was successfully used to measure the *Helicobacter pylori* of the Aptamer-MIP as substrate.

Helicobacter pylori is a gram-negative, microaerophilic bacterium that causes stomach ulcers that eventually lead to adenocarcinoma (stomach cancer) in later stages. The diagnosis of *Helicobacter pylori* has become of considerable interest because of its ability to cause gastric cancer. Gastric cancer mortality rates have risen sharply in recent years [29]. Therefore, there is a need for an effective method of detecting *Helicobacter pylori* in the early stages. That's why early detection of *Helicobacter pylori* is so important. There are ways to detect *Helicobacter pylori,* but they take a long time and cost a lot. To overcome these disadvantages, sensors with high sensitivity, low detection, and high selectivity are required [30].

The CN@IrCu acts as an excellent substrate with a rich functional group and high surface area for bonding and fixing aptamer on the surface of SPCE. This work has good selectivity against disturbances and this is one of the best advantages of the proposed system it is also the first design of CN@IrCu for electrochemical Aptamer-MIP application for detection of *Helicobacter pylori*.

EXPERIMENTAL

Materials and Apparatus

All chemicals used in this study were of high purity and also double distilled water was used. The $FeCl_3.6H_2O$, Tween 20, and dopamine were bought from Sigma-Aldrich. The $Cu(Cl)_2.3H_2O$, $Ir(Cl)_2$, HCl, NaOH, KCl, $MgCl_2$, Tris-HCl, and L-ascorbic acid were purchased from Merk. For electrochemical work, the solution containing the $Fe(CN)_6^{3-/4-}$ at a ratio of 1:1 and 0.1 mol^{-1} KCl was used. The *Staphylococcus aureus, Campylobacter jejuni, Vibrio cholerae, Staphylococcus aureus, Campylobacter fetus, and Helicobacter pylori were prepared in the* biological *laboratory of Ilam University.*

The sequence of aptamer was as follows: 5'AGTGTGCTCTTCTCAGGTCTCGGCGCGGTTGTGG GTACCTAGGGTTGTTGTTGCTTCTCAGCAGTGTCTC AGCATACGCA-3' [31].

The EIS, CV, and DPV were achieved with μ-AUTOLAB type ΙΙΙ computer controlled Potentiostat/Galvanostat (ECO-Chemie, Switzerland). The platinum wire as the counter electrode, the Ag/AgCl electrode as the reference, and SPCE (3 mm in diameter) as a working electrode were used. The characterization and structure of the CN@IrCu were carried out using Field Emission Scanning Electron Microscopy (FE-SEM; TSCAN, Czechia), Brunauer Emmett Teller (BET; Bruker-; Model-Belsorp miniII), and Fourier Transform Infrared Spectroscopy (FTIR; Bruker-; Model-VERTEX 70).

Bacteria Preparation

The *Helicobacter pylori* and *Campylobacter jejuni, Vibrio cholerae, Staphylococcus aureus, and Campylobacter fetus* were cultured in tryptone soy broth and the concentration of media was adjusted to 0.5 McFarland. The phosphate buffer was used to dilute the *Helicobacter pylori.*

The Preparation of CN Nanocapsules

In order to prepare the Fe_2O_3 nanocapsules using a hydrothermal method, the first 100 ml of 0.2 M of $FeCl_3$ solution was stirred. Then 100 ml of 5.4 M NaOH was added dropwise to the mentioned solution. In the next step, the mentioned solution was kept above for 75 min in the same conditions. Then the solution was transferred to the autoclave. The autoclave was kept for 96 h in the oven at a temperature of 100 °C. The product was centrifuged. The product was dried in an oven at 70 °C. The 320 mg of this product was dissolved in Tris-buffer solution and 160 mg of dopamine was added to it, and finally, it was steered for 3 h and the product was centrifuged and separated from the solvent and dried in an oven at 60 °C. The product was annealed at 500 °C for 3 h and then steered in 4 M HCl to remove the template. Then, in the last step, it was centrifuged (12000 rpm) and separated from the solvent to obtain the CN nanocapsule, and it was kept in an oven at 60 °C for drying.

Preparation of CN@IrCu Nanocapsule

To prepare the CN@IrCu nanocapsule, 50 mg of the previous synthetic material (CN nanocapsule) was ultrasonicated in 20 ml of water. Then, 1 ml of (60 mM) $IrCl_2$ and $CuCl_2$ were slowly added to the solution. For the final synthesis, L-ascorbic acid (1.00 ml) was added. In the last stage, it was centrifuged (12000 rpm) and separated from the solvent to obtain the synthetic substance, and the CN@IrCu nanocapsule was kept in an oven at 60 °C for drying.

Preparation of Aptamer-MIP

Before modification, the SPCE was pretreated using a potential of -0.4 to 1.5 V at 0.10 M HCl using a scan speed of 50 mV s^{-1} for 20 cycles [33]. Subsequently, different amounts of the CN@IrCu solution were dropped onto the surface of the bare SPCE and 5.0 µl was selected in the following experiments. The surface of CN@IrCu/SPCE was dried at room temperature. In TBST buffer (0.05% Tween 20, 10 mM Tris-HCl, pH = 7.4, 10 mM $MgCl_2$, and 10 mM KCl) 100 µl of 2 µM aptamer with 10^7 CFU ml^{-1} of *Helicobacter pylori* for 1 h at 37 ºC was incubated.

The Aptamer [*Helicobacter pylori*] complex was then placed on the modified electrode for 12 h to immobilize the electrode surface. In the next step, the *Helicobacter pylori* with a concentration of 10^7 CFU ml^{-1} was placed on the surface of the modified electrode for 30 min.

In the next step, for electro-polymerization dopamine was placed on the electrode surface in a 0.05 M dopamine monomer (pH = 7.4) solution to prepare MIP, and the CV in the range of -0.5 to 0.5 V during 13 cycles at the scan rate of 20 mV s^{-1} was applied [27]. The electrode was then immersed in the washing solution SDS 0.01M, and 5% HCl for 20 min. Then the DPV peak current changes were used to measure the bacteria. Incubation of *Helicobacter pylori* on the surface of the Aptamer-MIP/CN@IrCu/SPCE is due to the size of the holes in the surface of the electrode and the size of the *Helicobacter pylori*. A Schematic of the construction process of the Aptamer-MIP/CN@IrCu/SPCE is shown in Fig. 1.

RESULTS AND DISCUSSION

Surface Characterization

The morphological and composition analysis of the CN@IrCu was carried out using Raman, FTIR, MAP, BET, FESEM, EDX, and TGA.

The EDX spectra, EDX elemental mapping images, and SEM were used to study the morphology and structure of the CN@IrCu. As you can see in Figs. 2a-b, the Fe_2O_3 nanocapsules with uniform surface have been successfully made by hydrothermal method. Then, in the next step, the structure of the nanocapsule has been preserved after iron removal (Figs. 2c-d), and this is a sign of the successful

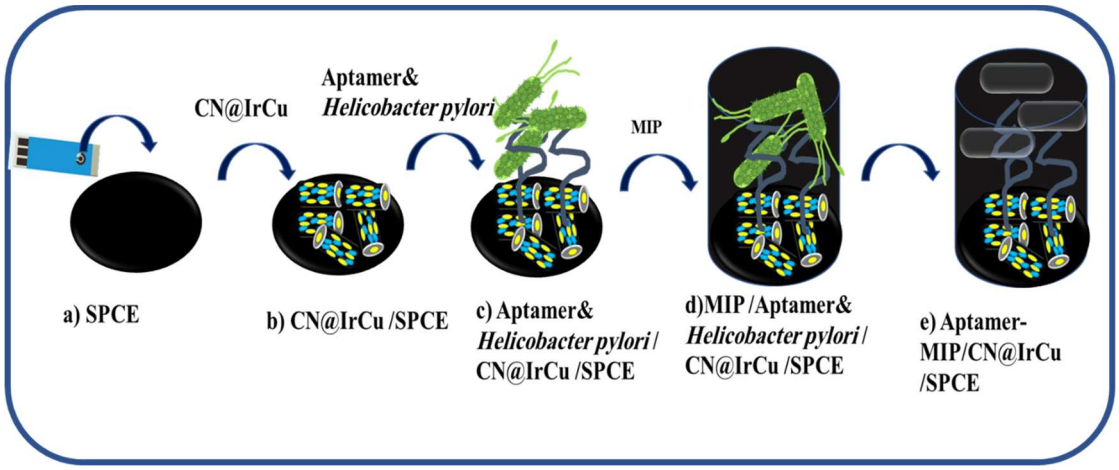

Fig. 1. Schematic of preparation of aptasensor for *Helicobacter pylori* measurement. (a) SPCE; (b) CN@IrCu/SPCE; (c) on Aptamer&*Helicobacter pylori*/CN@IrCu/SPCE; (d) MIP/Aptamer&*Helicobacter pylori*/CN@IrCu/SPCE; (e) Aptamer-MIP/CN@IrCu/SPCE.

synthesis of CN nanocapsules. Also, the average size of CN nanocapsules corresponds to the average size of Fe_2O_3 nanocapsules (about 650 nm). In Figs. 2e-f, the CN nanocapsules structure is preserved, and seems that its surface has become rougher after nano iridium and copper coating. The EDX spectra and EDX elemental mapping images of the CN@IrCu confirmed the presence of Ir, Cu, N, and C uniformly in the CN@IrCu (Fig. 3).

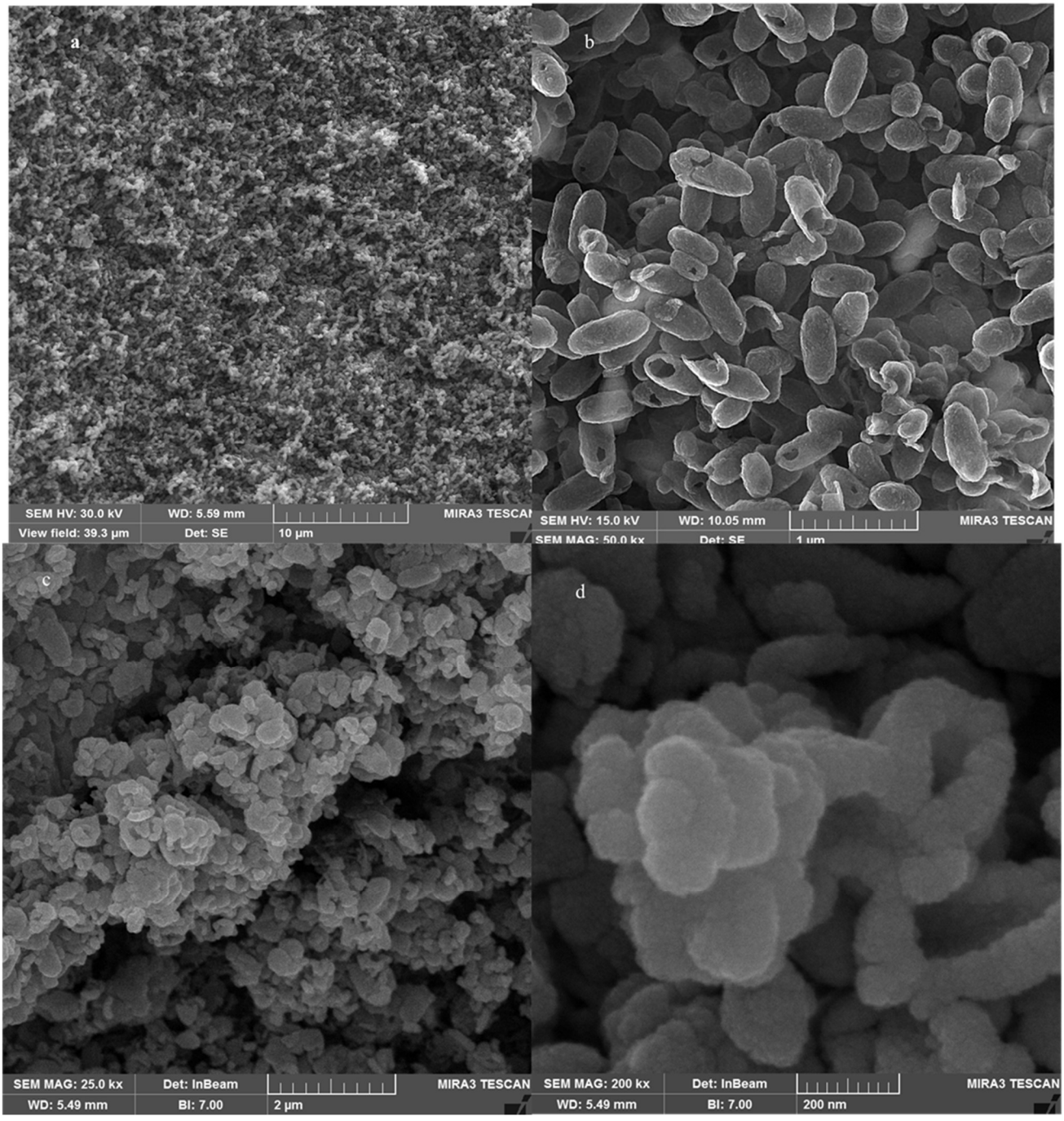

Fig. 2. (a) FE-SEM image of Fe_2O_3@CN, (b) NC, and (c,d) CN@IrCu.

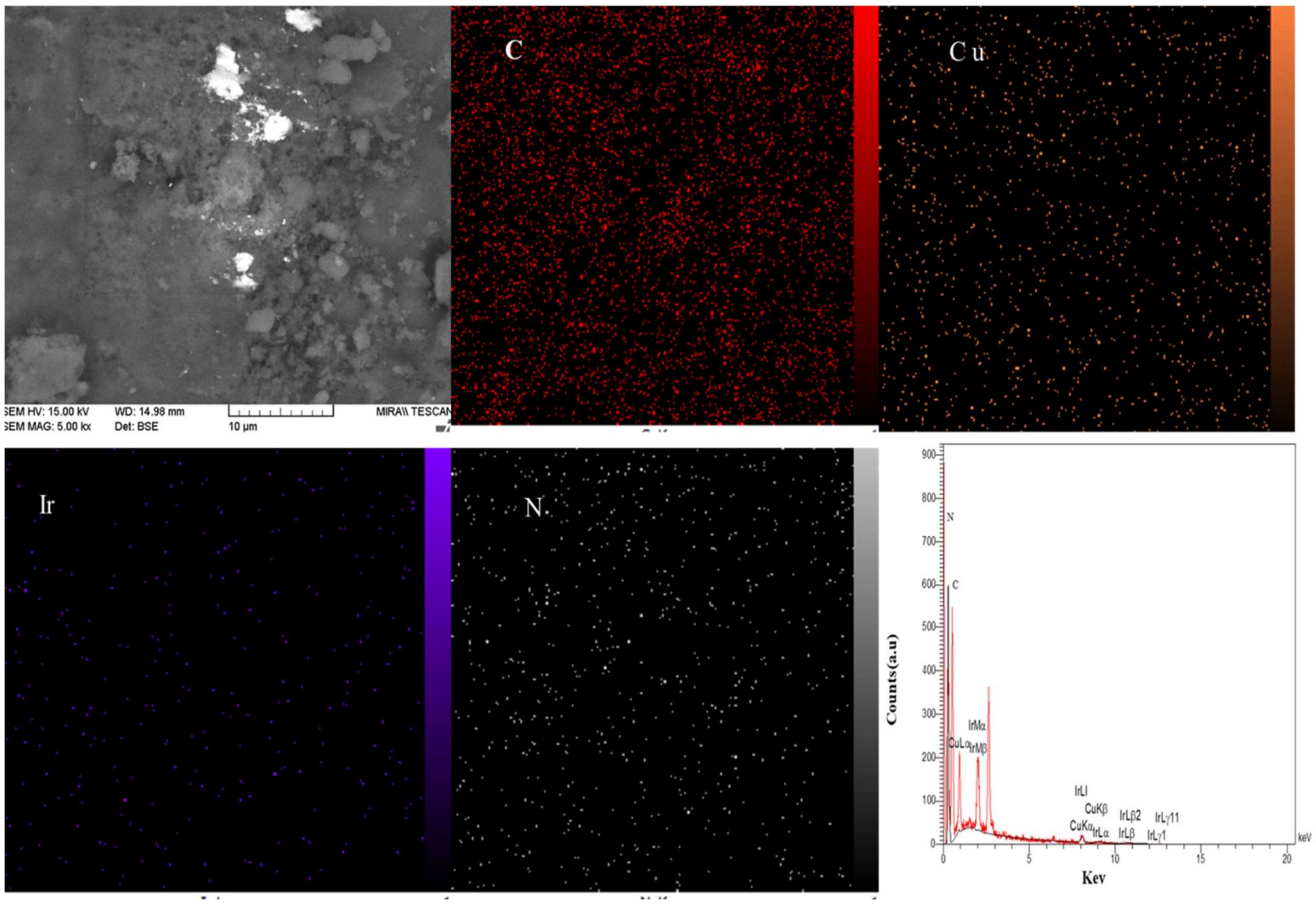

Fig. 3. EDS spectrum and EDS map of element distribution in the CN@IrCu.

The FTIR spectra of (a), (b) and (c) are related to Fe_2O_3 nanocapsule, CN nanocapsule, and CN@IrCu nanocapsule respectively (Fig. 1S(a)), the region 450-600 cm^{-1} is related to the Fe-O stretching, which indicates Fe_2O_3 nanocapsule successful synthesis. In the next step, after carbonation and removal of the Fe-O core, new peaks appeared which are characteristic of carbon and nitrogen compounds, and the region between 450-600 cm^{-1} was removed which indicates the removal of the Fe-O (Fig. 1S(b)). In the next step, after the formation of nano IrCu on CN nanocapsule, the peak area of 450-600 appeared, which indicates the successful synthesis of the formation of nano IrCu in CN nanocapsule Fig. 1S(c) [32].

The TGA curves related to CN nanocapsule (a) and CN@IrCu (b) are shown in Fig. 4A. As you can see, the TGA curve (a) begins to decompose at a temperature of 380 °C, and at a temperature above 580 °C, it burns completely, and the remaining weight is almost zero percent. The TGA curves of Fig. 4A (b) For CN@IrCu, it was found that the remaining 30% could be related to nano IrCu loading in the CN nanocapsule structure.

To further identify the composite structures, the Raman technique was applied. Figure 4B represents the red curve Raman spectra of CN and the green dash curve Raman spectra of CN@IrCu nanocapsules. The Raman pattern of CN confirms the presence of 1360 cm^{-1} of the D band and 1570 cm^{-1} of the G band that matched with the Raman spectra of carbon-based compounds [32]. After the IrCu nanoparticles formation on CN, an increment in the I_D/I_G peak ratios intensity of CN@IrCu (0.9) was observed compared with CN (0.75), confirming an increment in the edge defects due to the IrCu nanoparticles formation [33,34]. In addition, the surface area and pore size of the CN@IrCu were evaluated using N_2 adsorption and desorption isotherm

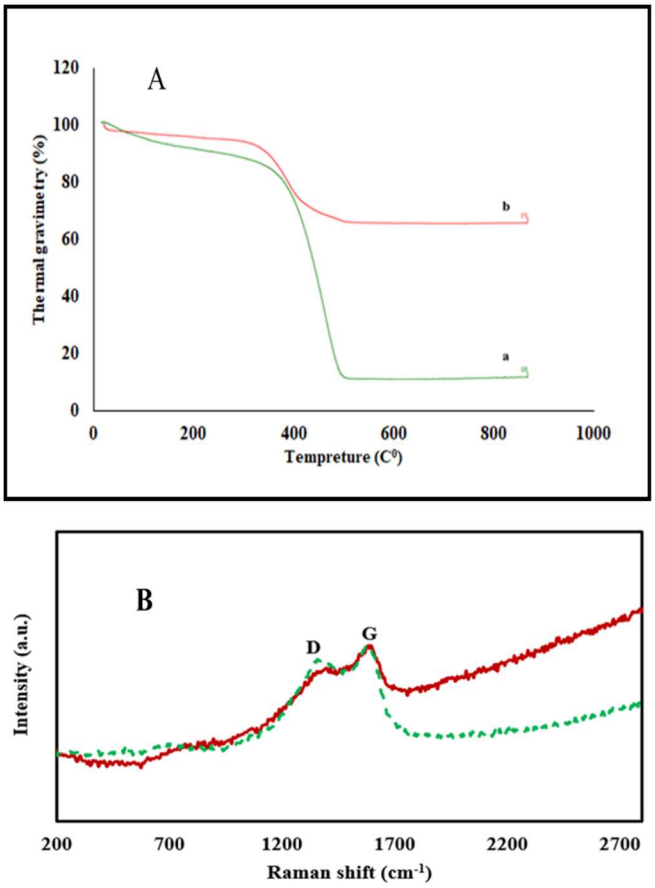

Fig. 4. (A) The TGA curve of (a) NC and (b) CN@IrCu. (B). The Raman spectra of NC (red curve) and CN@IrCu (green dash curve) nanocapsules.

and the pore size distribution diagram (Fig. 1S). The BET was used to study CN@IrCu surface area. The BET surface area 111.11 m^2 g^{-1} for the CN@IrCu was obtained, which is a very good surface area for compounds IrCu-based carbon nanomaterials. The isotherm diagram is a type IV plot, which is characteristic of mesoporous compounds. Therefore, the composition of CN@IrCu is one of the mesoporous compounds (Fig. 2S). The pore size distribution of this CN@IrCu is 18 nm (Fig. 2S inset).

Electrochemical study of the electrode surface and all electrode modification steps were evaluated by CV and EIS techniques. The CV and EIS were performed in a solution containing 0.1 M KCl and 5 mM $[Fe(CN)_6]^{3-/4-}$ as a redox probe.

As shown in Fig. 5A (curve a), well-defined redox peaks of the probe show the SPCE. Modifying the electrode by CN@IrCu reduces the current peak relative to the bare SPCE (Fig. 5A, curve b). In the next step, the peak current of the $[Fe(CN)_6]^{3-/4-}$ probe is reduced by placing aptamer [*Helicobacter pylori*], which may be due to the fact that the aptamer [*Helicobacter pylori*] has been successfully placed on the surface of the electrode (Fig. 5A, curve c). Another reason could be that the repulsion between the negatively charged $[Fe(CN)_6]^{3-}$/$[Fe(CN)_6]^{4-}$ redox probe and the negatively charged phosphate groups in the aptamer has reduced the peak current. In the next step, when the electro-polymerization electrode was applied on the

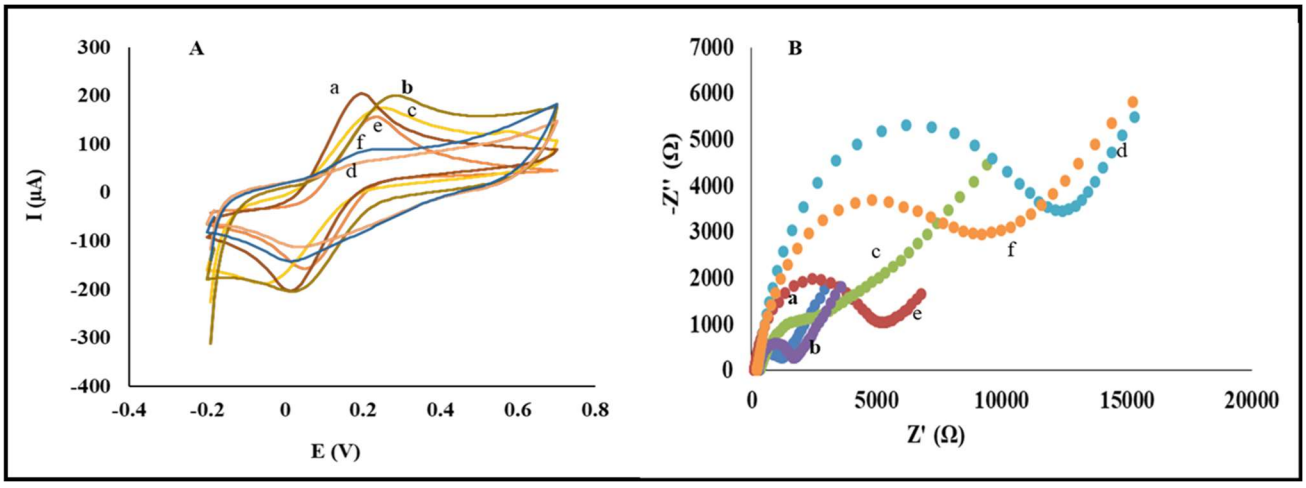

Fig.5. (A) CV and (B) EIS measurements of (a) SPCE, (b) CN@IrCu/SPCE (c) Aptamer&*Helicobacter pylori*/CN@IrCu /SPCE, (d) Dopamine/Aptamer&*Helicobacter pylori*/CN@IrCu/SPCE, (e) Aptamer-MIP/CN@IrCu/SPCE, (f) incubation of *Helicobacter pylori.*

Aptamer&*Helicobacter pylori*/CN@IrCu/SPCE surface, the peak current intensity was sharply reduced (Fig. 5A, curve d). In the next step, after washing the peak current increased (Fig. 5A, curve e). This is because *Helicobacter pylori* is separated from the electrode surface, creating a hole in the electrode surface and facilitating electron transfer. Another reason may be that some of the polymer dissolves in the washing solution. But current the peak current Aptamer-MIP /CN@IrCu/SPCE is less than Aptamer&*Helicobacter pylori* /CN@IrCu/SPCE, which confirms the polymer after washing on the surface.

After adding *Helicobacter pylori* to the Aptamer-MIP/CN@IrCu/SPCE surface, because the *Helicobacter pylori* was the same size as the surface of the hole on the surface of the electrode, the current peak is reduced, which indicates the successful design of the sensor (Fig. 5A, curve f).

The EIS is another technique in that the change in the values of Rct for different modified electrodes was chosen to study the surface properties during the fabrication process of Aptamer-MIP/CN@IrCu/SPCE. Figure 5B shows in a scan rate 100 mV s^{-1}, containing solution 0.1 M KCl and 5 mM $[Fe(CN)_6]^{3-/4-}$ the EIS of (a) SPCE, (b) CN@IrCu/SPCE (c) Aptamer&*Helicobacter pylori*/CN@IrCu/SPCE, (d) Dopamine/Aptamer&*Helicobacter pylori*/CN@IrCu/SPCE, (e) Aptamer-MIP/CN@IrCu/SPCE, (f) incubation of *Helicobacter pylori*. As shown in Fig. 5B (curve a), the Rct shows the SPCE. Modifying the electrode by CN@IrCu increased the Rct relative to the bare SPCE (Fig. 5B, curve b). In the next step, the Rct of the $[Fe(CN)_6]^{3-/4-}$ is increased by placing aptamer [*Helicobacter pylori*] (Fig. 5B, curve c). In the next step, when the electro-polymerization electrode was applied on the Aptamer&*Helicobacter pylori* /CN@IrCu/SPCE surface, the Rct was sharply increased (Fig. 5B, curve d) . In the next step, after washing the Rct decreased. After adding *Helicobacter pylori* to the Aptamer-MIP/CN@IrCu/SPCE surface, the Rct is increased (Fig. 5B, curve f). The EIS confirmed all CV behaviors and this is a sign of successful synthesis of Aptamer-MIP/CN@IrCu /SPCE.

Bacterial Detection

To evaluate the sensitivity and limit of detection (LOD) of the proposed aptasensor (Aptamer-MIP/CuIr@NC /SPCE), different concentrations including 10^2 CFU ml^{-1} to 10^7 CFU ml^{-1} for 25 min and the DPV technique was used to determine *Helicobacter pylori.* The optimized time and sensor incubation is shown in Fig. 3S. As shown in the Fig. 6. the current decreased with increasing concentration. Because the bacteria are in the cavity, it makes it difficult to transfer electrons between the Aptamer-MIP/CN@IrCu /SPCE and the $[Fe(CN)_6]^{3-/4-}$.

As can be seen, in Fig. 6. the calibration curve showed a good linear relationship between the peak current and the logarithm of the *Helicobacter pylori* concentration in the range of 10^2 CFU ml^{-1} to 10^7 CFU ml^{-1}. The linear

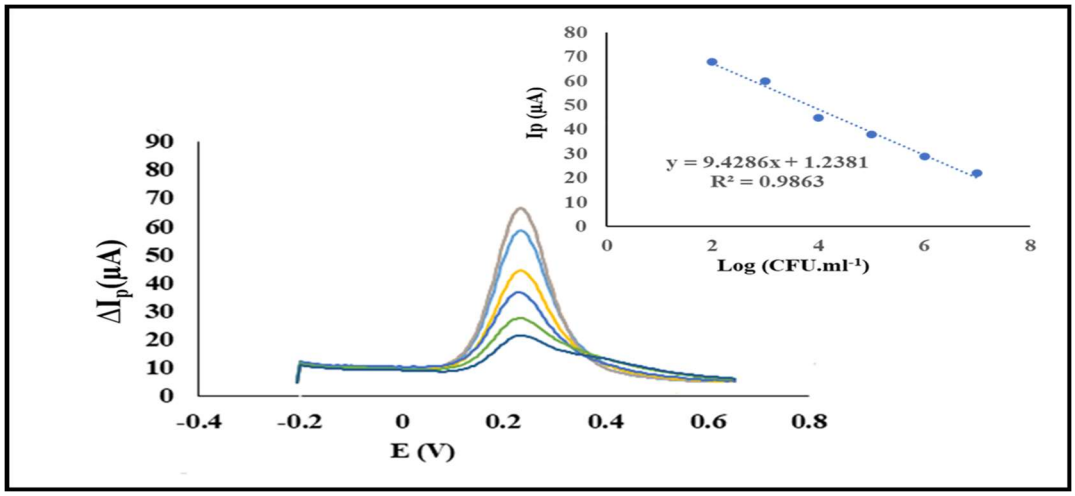

Fig. 6. DPV responses after incubating with different concentrations from 10^2 to 10^7 CFU ml^{-1} of the *Helicobacter pylori* in 0.1 M KCl and 5 mM $[Fe(CN)_6]^{3-/4-}$.

relationship could be represented by the equation, $I_P/\mu A$ = 9.428 log [*Helicobacter pylori]* (CFU ml^{-1}) +1.2381 with a correlation coefficient of 0.9863 and the limit of detection (LOD) (at signal to noise ratio of 3) 33 CFU ml^{-1}.

Repeatability, Reproducibility, Selectivity, and Stability of the Aptamer-MIP/CN@IrCu/SPnCE Sensor

The interferers such as *Campylobacter jejuni, Vibrio cholerae, Staphylococcus aureus, and Campylobacter fetus* at a concentration of 10^4 CFU ml^{-1} was used to evaluate the selectivity of *Helicobacter pylori*. The performance of the sensor was examined. As you can see in Fig. 4S, the Aptamer-MIP/CN@IrCu/SPCE has a high selectivity. Four electrodes were prepared to evaluate the reproducibility under the same conditions. As you can see in Fig. 5S(A), the relative standard deviation (RSD) of 4.94% was calculated and confirmed the repeatable results.

Also, to check the repeatability effect, a response to a concentration of 10^4 CFU ml^{-1} of bacteria was repeated four times by an electrode and showed reliable results Fig. 5S(B). The CV technique was used to evaluate the stability test. After fifty cycles of current changes, it was less than 5%, which is an indication of the stability of the Aptamer-MIP/ CN@IrCu/SPCE Fig. 6S.

Real Sample Preparation

To evaluate the performance of the sensor in the real sample, its application in the serum sample was investigated. The standard addition method was used for the real sample. The serum samples were diluted three times. Different concentrations of bacteria were first prepared with 0.5 McFarland and then added to diluted blood samples. The samples were examined by the DPV technique. As you can see in Table 1S, get acceptable results.

CONCLUSION

This paper was the first to use an Aptamer-MIP hybrid to detect *Helicobacter pylori*. The Aptamer-MP hybrid, a simple, fast, sensitive, and new Aptamer-MIP/CN@IrCu /SPCE-based electrochemical sensor was used to detect the selectivity of *Helicobacter pylori* with excellent detection. This method confirmed that the Aptamer-MIP hybrid was improved over the aptamer and MIP alone. These connection properties are dual detection of MIP and aptamer. The CN@IrCu plays a fundamental role in the structure of the sensor and was used as a suitable substrate for aptamer stabilization, leading to better detection of *Helicobacter pylori*. In addition to improving stability, the presence of CN@IrCu provides unique properties such as high surface area, and good chemical stability. In addition, this sensor showed an acceptable and satisfactory diagnostic limit in the serum sample. In the end, it can be said that this design can be used for other bacteria detection.

ACKNOWLEDGMENT

This research work was supported by the research facilities of Ilam University, Ilam, Iran**.**

REFERENCES

[1] Y. Panahi, A. Motaharian, M.R.M. Hosseini, O. Mehrpour, Sens. Actuators B Chem. 273 (2018) 1579.
[2] S. Sadeghi, M. Hemmati, A. Garmroodi, Electroanalysis 25 (2013) 316.
[3] J.P. Hart, A. Crew, E. Crouch, *et al*., Anal. Lett. 37 (2004) 789.
[4] R.E Wang, H. Wu, Y. Niu, J. Cai, Curr. Med. Chem. 18 (2011) 4126.
[5] X.T. Ma, X.W. He, W.Y. Li, Y.K. Zhang, Talanta 191 (2019) 222.
[6] K. Gokulakrishnan, T. Prakasam, Arab. J. Chem. 9 (2016) S528.
[7] D. Cai, L. Ren, H. Zhao, C. Xu, L. Zhang, Y. Yu, H. Wang, Y. Lan, M.F. Roberts, J.H. Chuang, M.J. Naughton, Z. Ren, T.C. Chiles, Nat. Nanotechnol. 5 (2010) 597.
[8] D. Li, Z. Bie, F. Wang, E. Guo, Analyst 143 (2018) 4936.
[9] D. Li, T. Tu, X. Wu, Anal. Methods 10 (2018) 4419.
[10] D. Li, T. Tu, M. Yang, C. Xu, Talanta 184 (2018) 316.
[11] D. Li, N. Wang, F. Wang, Q. Zhao, Anal. Methods 11 (2019) 3212.
[12] D. Li, S. Zhai, R. Song, Z. Liu, W. Wang, Spectrochim. Acta A Mol. Biomol. 227 (2020) 117542.
[13] C.J. Tan, S. Wangrangsimakul, R.B. Bai, Y.W. Tong,

Chem. Mater. 20 (2008) 118.
[14] K. Haupt, K. Mosbach, Chem. Rev. 100 (2000) 2495.
[15] F.G. Tamayo, E. Turiel, A. Martin-Esteban, J. Chromatogr. A 1152 (2007) 32.
[16] N. Kirsch, J. Hedin-Dahlstrom, H. Henschel, M.J. Whitecombe, S. Wikman, I.A. Nicholls, J. Mol. Catal. B: Enzym. 58 (2009) 110.
[17] E.L. Holthoff, F.V. Bright, Anal. Chem. Acta 594 (2007) 147.
[18] M. Li, X. Lin, Z. Xie, J. Chromatogr. A 1216 (2009) 5320.
[19] D. Cunliffe, A. Kirby, C. Alexander, Adv. Drug Deliv. Rev. 57 (2005) 1836
[20] W. Yang, W. Zhou, W. Xu, H. Li, W. Huang, B. Jiang, Z. Zhou, Y. Yan, J. Chem. Eng. Data 57 (2012) 1713.
[21] A. Poma, H. Brahmbhatt, H.M. Pendergraff, J.K. Watts, N.W. Turner, Adv. Mater. 27 (2015) 750.
[22] Z. Mokhtari, H. Khajehsharifi, S. Hashemnia, Z. Solati, R. Azimpanah, S. Shahrokhian, Sens. Actuators B (2020) 128316.
[23] N.M. Danesh, H.B. Bostan, K.H. Abnous, M. Ramezani, K. Youssefi, S.M. Taghdisi, G.H. Karimi, a review, TrAC Trends Anal. Chem. 99 (2018) 117.
[24] M. Roushani, F. Shahdost-fard, Bioelectrochemistry 126 (2019) 38.
[25] X. Qiao, K. Li, J. Xu, N. Cheng, Q. Sheng, W. Cao, J. Zheng, Biosens. Bioelectron. 113 (2018) 142.
[26] W. Bai, N.A. Gariano, D.A. Spivak, J. Am. Chem. Soc. 135 (2013) 6977.
[27] A. Poma, H. Brahmbhatt, H.M. Pendergraff, J.K. Watts, N.W. Turner, Adv. Mater. 27 (2015) 750.
[28] W. Bai, D.A. Spivak, Angew. Chem. 126 (2014) 2127.
[29] S. Guptaa, A. Tiwarib, U. Jaina, N. Chauhan, Mater. Sci. Eng. C 103 (2019) 1097 33
[30] Z. Liu, X. Su, Biosens. Bioelectron. 87 (2017) 66-72.
[31] L. Gu, W. Ren, X. Ma, M. Qin, M. Lyu, S. Wang, Helicobacter 24 (2019) 12577.
[32] M. Sarabaegi, M. Roushani, H. Hosseini, Talanta 223 (2021) 121700.
[33] H. Hosseini, M. Roushani, Chem. Eng. J. 402(2020) 126174.
[34] M. Roushani, H. Hosseini, Z. Hajinia, Z. Rahmati, Electrochim. Acta 388 (2021) 138608.